



Heat fluxes at the Earth's surface and core–mantle boundary since Pangea formation and their implications for the geomagnetic superchrons

Nan Zhang^{*}, Shijie Zhong

Department of Physics, University of Colorado, Boulder, CO 80309, United States

ARTICLE INFO

Article history:

Received 6 January 2011

Received in revised form 29 March 2011

Accepted 2 April 2011

Available online 5 May 2011

Editor: Y. Ricard

Keywords:

mantle convection

heat flux

supercontinent Pangea

magnetic polarity reversals

ABSTRACT

The Earth's surface and core–mantle boundary (CMB) heat fluxes are controlled by mantle convection and have important influences on Earth's thermal evolution and geodynamo processes in the core. However, the long-term variations of the surface and CMB heat fluxes remain poorly understood, particularly in response to the supercontinent Pangea – likely the most significant global tectonic event in the last 500 Ma. In this study, we reconstruct temporal evolution of the surface and CMB heat fluxes since the Paleozoic by formulating three-dimensional spherical models of mantle convection with plate motion history for the last 450 Ma that includes the assembly and break-up of supercontinent Pangea. Our models reproduce well present-day observations of the surface heat flux and seafloor age distribution. Our models show that the present-day CMB heat flux is low below the central Pacific and Africa but high elsewhere due to subducted slabs, particularly when chemically dense piles are present above the CMB. We show that while the surface heat flux may not change significantly in response to Pangea assembly, it increases by ~16% from 200 to 120 Ma ago as a result of Pangea breakup and then decreases for the last 120 Ma to approximately the pre-200 Ma value. As consequences of the assembly and breakup of Pangea, equatorial CMB heat flux reaches minimum at ~270 Ma and again at ~100 Ma ago, while global CMB heat flux is a maximum at ~100 Ma ago. These extrema in CMB heat fluxes coincide with the Kiaman (316–262 Ma) and Cretaceous (118–83 Ma) Superchrons, respectively, and may be responsible for the Superchrons.

© 2011 Elsevier B.V. All rights reserved.

1. Introduction

Heat fluxes at the Earth's surface and core–mantle boundary (CMB) have important influences on Earth's thermal evolution and geodynamo processes in the core (Aubert et al., 2008; Davies, 1999; Lay et al., 2008). It is generally agreed that the total surface heat flux for the present-day is ~44 TW, of which ~8 TW comes from the radiogenic heating in continental crust and ~36 TW is due to mantle convection process (e.g., Davies, 1999). The total surface heat flux is predominated by heat loss on sea floors, due to both their larger surface areas and larger averaged heat flux than those for continents (Fig. 1a) (Pollack et al., 1993). Oceanic heat flux is highest at the mid-ocean ridges and decreases with increasing distance from the ridges. This spatial distribution can be related to the age distribution of the oceanic floor (Fig. 1b) and explained by a half-space cooling model (e.g., Lister, 1977). However, time evolution of the surface heat flux is not well understood even for the most recent geological history associated with supercontinent Pangea. Grigne et al. (2005) suggested that the present-day heat flux is at its peak since Pangea breakup at ~180 Ma ago, because Pangea breakup leads to shorter-wavelength

convection that transfers heat more efficiently. However, contrary to Grigne et al.'s (2005) proposal, Loyd et al. (2007) and Becker et al. (2009) showed that the total surface heat flux has decreased for the last 140 Ma at a rate of ~0.2% every million years, using plate reconstruction models that are available for back to the Cretaceous (i.e., ~140 Ma) (e.g., Müller et al., 2008). However, there has been no attempt to reconstruct surface heat flux history prior to Pangea breakup.

CMB heat flux controls thermal evolution of the core, and has long been suggested to play a crucial role in powering the geodynamo (e.g., Buffett, 2002; Davies, 1999). Based on geodynamo modeling, Olson et al. (2010) suggest that global CMB heat flux and CMB heat flux in the equatorial regions may control the geomagnetic polarity reversals and may be the key to understanding the causes for the long-term (tens of millions of years) stable polarities such as the Kiaman and Cretaceous Superchrons that occurred during the time periods of 316–262 Ma and 118–83 Ma ago, respectively (Cande and Kent, 1995; Olson and Glatzmaier, 1996). An unstable (stable) geomagnetic polarity occurs when CMB heat flux or equatorial CMB heat flux is high (low) (Olson et al., 2010). Several methods have been used to estimate CMB heat flux. Davies (1988) and Sleep (1990) used the swell topography and plate motions (i.e., plume buoyancy flux) to constrain the total CMB heat flux to be ~3.5 TW or ~10% of the total surface convective heat flux, but more realistic model calculations (Leng and Zhong, 2008;

^{*} Corresponding author.

E-mail addresses: nan.zhang@colorado.edu (N. Zhang), szhong@colorado.edu (S. Zhong).

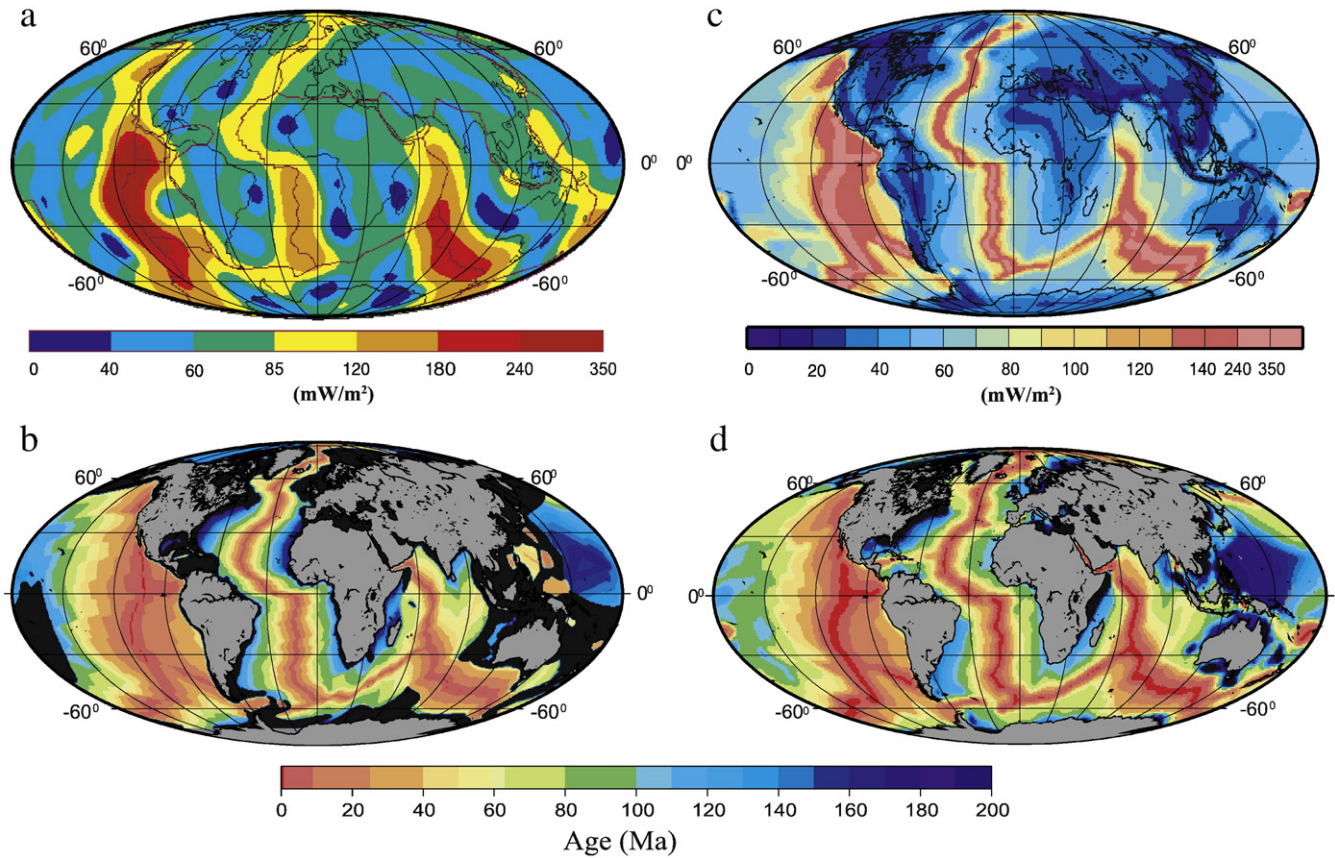


Fig. 1. The observed present-day surface heat flux (a) (Pollack et al., 1993), seafloor age distribution (b) (Müller et al., 1997), the model present-day surface heat flux (c) and seafloor age distribution (d) for case HF1.

Zhong, 2006) suggested that the total CMB heat flux is ~ 12 TW, due to adiabatic cooling effects on plume buoyancy flux. The latter is broadly consistent with that inferred from the perovskite to post-perovskite phase change studies (Hernlund et al., 2005; Lay et al., 2008). Also, the present-day seismic structure has been used as a proxy for spatial distribution of CMB heat flux in geodynamo studies (Aubert et al., 2008; Olson et al., 2010; Olson and Glatzmaier, 1996). However, to apply geodynamo models to understand geomagnetic polarity reversals such as the Kiaman and Cretaceous Superchrons, it is necessary to formulate models of CMB heat flux that consider geological history back to Pangea era (~ 330 Ma ago).

The surface and CMB heat fluxes are controlled by mantle convection. Although mantle convection models have been formulated to constrain time evolution of mantle structures and to interpret mantle seismic structure (e.g., Bunge et al., 1998; McNamara and Zhong, 2005; Zhong et al., 2007) and surface vertical motion history (e.g., Liu et al., 2008; Moucha et al., 2008), no such attempts have been made to reconstruct the surface and CMB heat flux history. A difficulty in reconstructing mantle convection and heat flux history back to the Pangea era is the lack of constraints on plate motion history for the Paleo-Pacific Ocean before 120 Ma (e.g., Lithgow-Bertelloni and Richards, 1998), although continental plate motions in the African hemisphere are well constrained since the Paleozoic as in the assembly and breakup of Pangea (e.g., Scotese, 2001). In a recent study (Zhang et al., 2010), we constructed a proxy global plate motion for the last 450 Ma to examine the effects of Pangea on mantle structure evolution, and showed that our models with this global plate motion model reproduce the present-day seismic structure significantly better than the models with only 120 Ma plate motion history (Bull et al., 2009; McNamara and Zhong, 2005).

The main goal of this study is to reconstruct the surface and CMB heat flux history since the Paleozoic, using mantle convection models

with the plate motion history model (Zhang et al., 2010). We are particularly interested in understanding how Pangea assembly and breakup influence the surface and CMB heat fluxes and their implications for the thermal evolution of the mantle and geomagnetic field. This paper is organized as follows. Section 2 describes mantle convection models with the plate motion history for the last 450 Ma. Section 3 presents model results. Discussions and conclusions are presented in Sections 4 and 5.

2. Methods and models

Our three-dimensional spherical models of mantle convection with the last 450 Ma plate motion history are the same as that in Zhang et al. (2010). Here we only describe the most important aspects of the models. Our models assume an infinite Prandtl number and the Boussinesq approximation. The conservation equations of the mass, momentum, and energy, and the advection equation of compositions are described in Zhong et al. (2008). The material properties and thermodynamic constants are shown in Table 1. The models consider a mixed heating mode with heating from both below and within the mantle, and employ temperature- and depth-dependent viscosity with a relatively weak upper mantle. Some model calculations also include phase changes of Ringwoodite to perovskite and perovskite to post-perovskite.

Our models have five controlling parameters: internal heat generation rate H , buoyancy number B , Rayleigh number Ra , temperature- and depth-dependent viscosity η , and surface plate motions (Zhang et al., 2010). Nondimensional internal heat generation rate $H = QR^2/\kappa\Delta T$, buoyancy number $B = \Delta\rho/\alpha\rho\Delta T$, temperature- and depth-dependent viscosity $\eta = \eta_0(r)\exp[E(0.5-T)]$, and Rayleigh number $Ra = \rho g\alpha\Delta TR^3/\kappa\eta_0$, where Q , ρ , κ , and α are the volumetric heat generation rate, density, thermal diffusivity, and coefficient of thermal expansion of the mantle,

Table 1
Material properties and constants.

Parameters	Value
Earth's radius, R	6370 km
Gravitational acceleration, g	$9.8 \text{ m}\cdot\text{s}^{-2}$
Mantle density, ρ	$3300 \text{ kg}\cdot\text{m}^{-3}$
Thermal diffusivity, κ	$10^{-6} \text{ m}^2\cdot\text{s}^{-1}$
Coefficient of thermal expansion, α	$2 \times 10^{-5} \text{ K}^{-1}$
Temperature difference, ΔT	2500 K
Thermal conductivity, k	$4 \text{ Wm}^{-1} \text{ K}^{-1}$
Clapeyron slope for the 670 km phase boundary	–3 MPa/K
Density jump across the 670 km phase boundary	8%
Clapeyron slope for the 2700 km phase boundary	8 MPa/K
Density jump across the 2700 km phase boundary	1.5%

respectively, ΔT is the temperature difference across the mantle, $\Delta \rho$ is the density difference between the background mantle and the chemical pile above the CMB, η_r is the reference viscosity and is the lower mantle viscosity at mean mantle temperature, g is the gravitational acceleration, R is the Earth's radius, $\eta_0(r)$ is the depth-dependent pre-factor, and T and E are the non-dimensional temperature and activation energy, respectively. In our calculations, H is set to be 100, which yields ~60% internal heating ratio for most cases, and E is 9.21, giving rise to viscosity variations of 10^4 due to temperature variations. The lower mantle viscosity is ~60 times higher than that for the upper mantle for most cases (Hager and Richards, 1989), but this viscosity contrast is also varied to study its effects. Details of the model parameters are presented in Table 2.

Our global plate motion model for the last 450 Ma consists of 34 different stages and was fully described in Zhang et al. (2010). Our plate motion model for the last 120 Ma uses the published model by Lithgow-Bertelloni and Richards (1998) and Ricard et al. (1993). For plate motions before 120 Ma, our model considers realistic continental plate motions in the African hemisphere, but for plate motions in the Pacific hemisphere, plate configurations are assumed to resemble those at 120 Ma ago with divergent plate motions and averaged speed of ~8 cm/yr. We note that in the plate motion model for the last 120 Ma (e.g., Lithgow-Bertelloni and Richards, 1998), the Pacific plates have an averaged speed ranging from 7 to 8 cm/yr, except for a period between 120 Ma and 80 Ma ago with significantly larger plate motions that reach ~12 cm/yr at ~95 Ma. However, this time period with large plate motions coincides with the Cretaceous Superchron, making the large plate motions not as well constrained (e.g., Heller et al., 1996; Rowley, 2002; Cogné and Humler, 2004). The assumed divergent plate motions in the Pacific since the Paleozoic are supported by geological evidence of accretionary terrains of oceanic origins along the Pacific rims (e.g., Safonova et al., 2009), and also by our study (Zhang et al., 2010)

showing that the present-day seismic structure is reproduced significantly better with divergent plate motions for the Pacific for the last >300 Ma, compared to that with the plate motion only for the last 120 Ma (Bull et al., 2009; McNamara and Zhong, 2005). In this study, we also vary magnitude of plate motions in the Pacific hemisphere before 120 Ma to examine its effects.

The non-dimensional radii for the top surface and bottom (i.e., CMB) boundaries are 1 and 0.55, respectively. Isothermal boundary conditions are applied at the surface and CMB in all calculations, and the fixed CMB temperature with time is justified because of the relatively small (i.e., ~70 K per Ga) mantle secular cooling (e.g., Davies, 1999). For velocity boundary conditions, the surface is prescribed with time-dependent velocity (i.e., plate motion) while the CMB is a free-slip boundary. All the cases start with one-dimensional initial temperature profiles derived from pre-calculations that use the same model parameters except that the plate motion boundary condition is replaced with a free-slip boundary condition. Ra is also chosen to be generally consistent with the imposed plate motion. While our modeling practice in choosing initial temperature profiles and Ra in our convection models with imposed plate motions is reasonable (e.g., McNamara and Zhong, 2005), we would also like to point out how plate tectonics and mantle convection are dynamically coupled together remains a challenging problem due to our poor understanding of plate boundary processes (e.g., Bercovici, 2003; King et al., 2002). For each model run, surface plate motions for the first stage (i.e., at 450 Ma ago) are employed for 150 Ma before the plate motions are updated with subsequent plate motion history (Zhang et al., 2010). Consequently, only model heat fluxes for the last ~400 Ma are interpreted in this study. The governing equations are solved with CitcomS (Zhong et al., 2000, 2008). For most cases, we use a grid with ~1,330,000 elements (i.e., 12×48^3 elements, see Zhong et al., 2000), but three higher resolution models are also computed (Table 2).

Considering the important effects of seafloor age on the surface heat flux (e.g., Lister, 1977; Parsons, 1982), we quantify seafloor age distribution at different times in our models. Seafloor age calculation is only dependent on the plate motion model, and is computed independently from mantle convection. In practice, we use the tracer advection functionality of CitcomS to compute the age. Initially, tracers with zero age are assigned to surface elements that have horizontal resolution of 34 km. The positions and ages of tracers are updated every time step based on a given time increment and the imposed plate motion history. At each time step, a fixed number of tracers with zero age are continuously added to elements at divergent plate boundaries where the positive divergence is greater than some threshold, and at the same time, tracers are removed at convergent plate boundaries with negative divergence. Seafloor age for each surface element is computed by averaging ages of all the tracers in that element, and the

Table 2
Input parameters and outputs for mantle convection models.

Case	Ra	Grids	η_{0lm}^a	B	I.C. & B.C. ^b	Phase depth ^c	(t_1, t_2) ^d	ξ (%) ^d	q_s (mW/m ²) ^d
HF1	2×10^8	12×64^c	2.0	0.5	IC1(BC1)	–	(272, 96)	62	73.7
HF1R	2×10^8	12×48^c	2.0	0.5	IC1(BC1)	–	(272, 97)	61	75
HF2	2×10^8	12×48^c	2.0	–	IC2(BC1)	–	(285, 130)	51	76.4
HF3	10^8	12×48^c	0.73	0.5	IC1(BC1)	–	(263, 101)	55	75.1
HF4	2×10^8	12×48^c	2.0	0.5	IC1(BC1)	2700 km	(268, 97.5)	56	74.8
HF5	2×10^8	$12 \times 48^b \times 64$	2.0	0.5	IC1(BC1)	670 km	(227, 98.5)	63	74.6
HF6	2×10^8	12×64^c	2.0	0.5	IC1(BC2)	–	(282, 99)	65	73.0

^a η_{0lm} is the pre-exponential factor for the viscosity equation for the lower mantle at 670 km depth. The pre-factors for the lithosphere (i.e., <100 km depth) and for the upper mantle between 100 km and 670 km depths are 1 and 0.0333, respectively, for all cases.

^b The symbols for initial and boundary conditions. Two different initial conditions, IC1 and IC2, and two boundary conditions, BC1 and BC2, are used. IC1 and IC2 use 1D temperature profiles from pre-calculations with free-slip boundary conditions with and without chemical piles, respectively. BC1 is for the average spreading rate of 8 cm/yr and BC2 represents the average spreading rate of 11 cm/yr for oceanic plates in the Pacific hemisphere before 119 Ma.

^c Clapeyron slopes for the perovskite to post-perovskite (2700 km) and the Ringwoodite to perovskite (670 km) phase changes are 8 MPa/K, and –3 MPa/K, respectively, and the density jumps across these two phase changes 1.5%, and 8%, respectively.

^d t_1 and t_2 are the times when the equatorial CMB heat flux reaches the minimum. ξ is the internal heating ratio. q_s is the present day surface heat flux.

elemental seafloor age is then projected to surface nodes to obtain the seafloor age distribution on a grid. The age of continental regions in our models is undetermined. Our forward modeling approach is different from previous efforts in deriving seafloor age distribution that often start from the present-day seafloor age distribution and integrate backwards on either regional or global scales (e.g., Conrad and Gurnis, 2003; Müller et al., 2008; Wen and Anderson, 1995; Xu et al., 2006). However, our forward-modeling approach is efficient in using with mantle convection models and may also help verify the plate motion model by comparing with present-day seafloor age distribution.

3. Results

In this section, we first present results of the surface and CMB heat fluxes for reference case HF1 (Table 2). We then examine the influences of different parameters including lower mantle viscosity, chemical piles, phase changes, and plate motions.

3.1. Surface heat flux for case HF1

We start with reference case HF1 that has Rayleigh number of 2×10^8 , and an initially 250 km thick chemical layer above the CMB with a buoyancy number B of 0.5 (Table 2). The global root-mean-square velocity for the imposed surface velocity varies between ~ 6.6 cm/yr and

4 cm/yr from the Paleozoic to the present-day (Fig. 2a). The pre-calculation for this case using free-slip boundary condition yields an average surface motion of 3.6 cm/yr, suggesting that the convective vigor or Ra is consistent with the surface plate motion. The depth-dependent pre-factor $\eta_0(r)$ are 1 and 1/30 for the lithosphere and upper mantle, respectively, and for the lower mantle, $\eta_0(r)$ increases linearly from 2.0 at the 670 km depth to 6.8 at the CMB (Table 2 and Fig. 3a) (Zhang et al., 2010). This leads to a mantle viscosity structure in which the lower mantle on average is ~ 2 orders of magnitude more viscous than the upper mantle (Fig. 3a). With $Ra = 2 \times 10^8$ and other parameters listed in Tables 1 and 2, the averaged viscosities for the upper mantle and lower mantle are $\sim 4.5 \times 10^{19}$ Pas and $\sim 7 \times 10^{21}$ Pas, respectively. The internal heating ratio for this case determined a posteriori from the surface and CMB heat fluxes is $\sim 61\%$ (Table 2), implying a significant but reasonable fraction of heating from the core (e.g., Bunge, 2005; Hernlund et al., 2005; Leng and Zhong, 2008; Zhong, 2006).

We first present the present-day surface heat flux from case HF1. The calculated present-day surface heat flux compares well with the observation (Fig. 1a and c). The calculated present-day average surface heat flux is 74 mW/m^2 (Fig. 2b) or 38 TW in total, which is slightly higher than the estimated 36 TW for the present-day mantle heat flux. Our model reproduced the observations of high heat flux at the mid-ocean ridges, and low heat flux in continental regions (Fig. 1c), although due to limited model resolution heat flux at some ridge

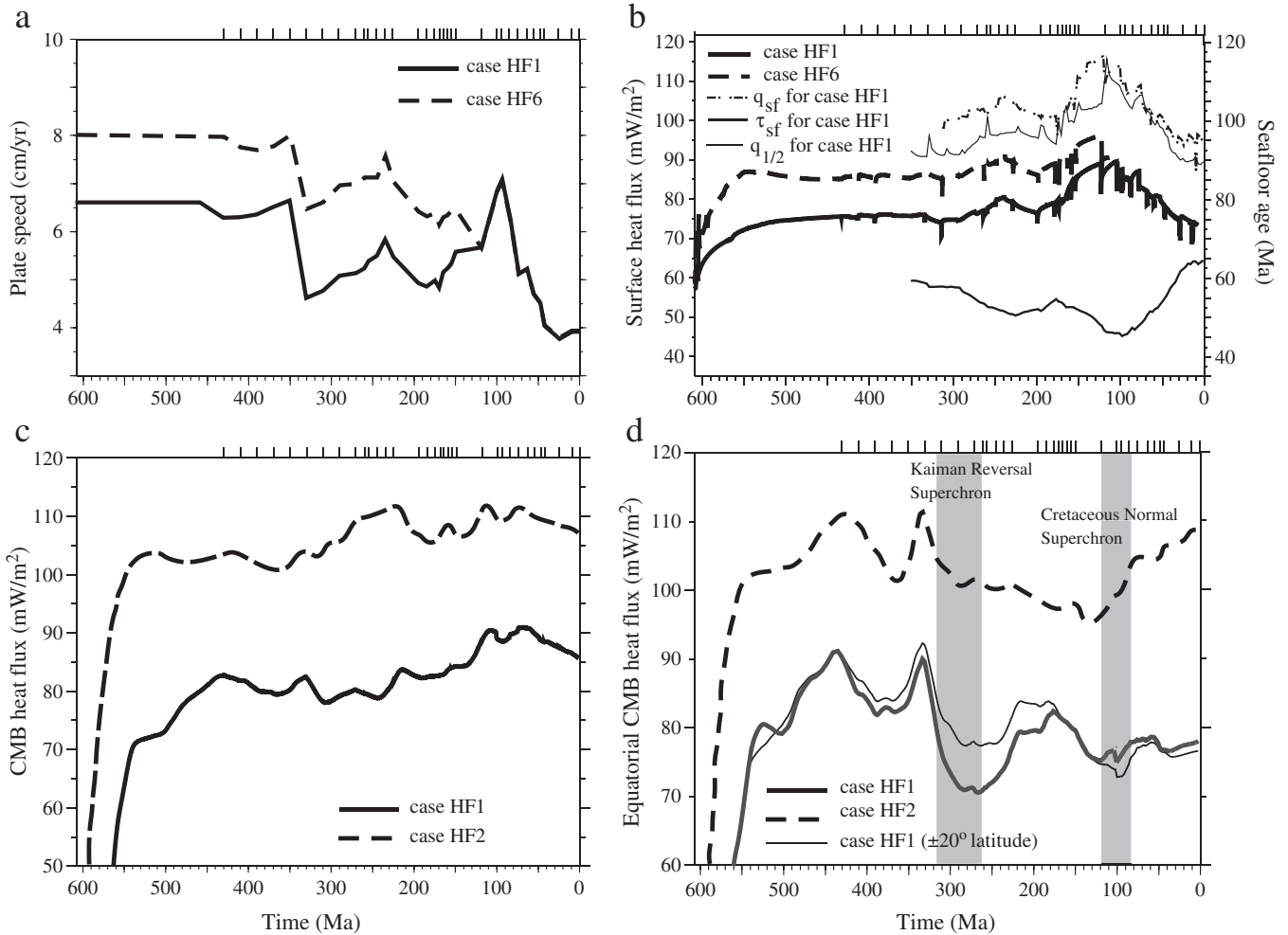


Fig. 2. Time dependence of (a) globally averaged plate motions for cases HF1 and HF6, (b) the globally averaged surface heat fluxes for cases HF1 and HF6, averaged heat flux, q_{sf} , and age, τ_{sf} , for seafloor younger than 160 Ma, and the predicted oceanic heat flux, $q_{1/2}$, based on the half-space cooling model for the case HF1, (c) the globally averaged CMB heat flux for cases HF1 and HF2, and (d) the equatorial CMB heat flux for cases HF1 and HF2. The tick mark on the top horizontal axis shows the time for updating every stage of plate motions. In Fig. 2d, equatorial CMB heat fluxes for case HF1 were computed for two latitude bands (10° and 20° on each side of the equator), and the two shaded zones represent the time periods for the Kaiman and Cretaceous Superchrons.

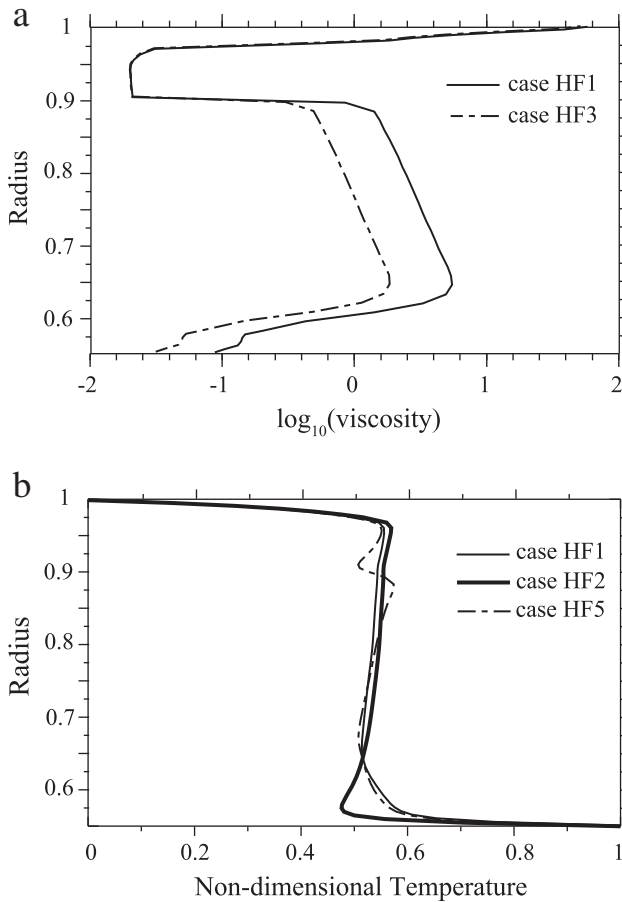


Fig. 3. Depth dependences of horizontally averaged mantle viscosities for cases HF1 and HF3 (a), and mantle temperatures for cases HF1, HF2, and HF5 (b).

segments appears too high. Our model did not include back-arc spreading plate motions, and consequently did not reproduce the observed heat flux highs there.

The averaged surface heat flux in general correlates positively with the plate motions (Fig. 2 a and b). Before Pangea assembly that occurred at 330 Ma ago, the surface heat flux shows little variation with time, similar to the plate motions. The surface heat flux distribution before Pangea formation is characterized by high heat flux in the oceanic areas (i.e., the Pacific hemisphere) and low heat flux in the continental areas (i.e., the African hemisphere) (Fig. 4g). From 330 Ma to 290 Ma ago, the average surface heat flux decreases slightly due to the collision between Laurussia and Gondwana at 330 Ma ago that leads to the disappearance of oceanic lithosphere between these two continents. After 290 Ma, the surface heat flux starts to increase due to the opening of the Tethys Ocean (Scotese, 2001; Zhang et al., 2010) (Fig. 4e). Both the surface heat flux and plate motion reach to peaks at ~240 Ma ago (Fig. 2b). After 240 Ma, Pangea grows gradually as it collides with the China blocks and Cimmeria (Turkey, Iran, and Tibet), causing oceanic regions to reduce and hence the global average plate motion and surface heat flux to decrease (Fig. 2a and b). At ~190 Ma ago, Pangea starts to break up, and new seafloors at the central Atlantic, Indian Ocean, South Atlantic, and North Atlantic are created from 190 Ma to 120 Ma (e.g., Fig. 4c). This leads to an increase in global plate motion and causes the global averaged surface heat flux to increase by ~16% during this period (Fig. 2a and b). For the last 120 Ma, as the oceanic plate motion decreases, the surface heat flux decreases steadily to approximately the pre-Pangea breakup value. It should be pointed out that the sudden changes in the averaged surface heat flux (Fig. 2b) are caused by sharp transitions of plate motions

from one time frame to the next in our plate motion model (Zhang et al., 2010).

The total oceanic heat flux is controlled by seafloor area-age distribution (e.g., Parsons, 1982). We computed the age distribution of oceanic lithosphere at different times based on the plate motion model used in case HF1 (Figs. 1d, 4d, f, and h). The present-day seafloor age distribution is consistent with the observed except for back-arc regions that were not considered in our models (Fig. 1b and d). The seafloor age distributions mostly reflect the seafloor spreading at various stages, for example, the young Atlantic and Indian Oceans at 110 Ma ago (Fig. 4d), and the Tethys Ocean at 200 Ma ago (Fig. 4f). We do not interpret the seafloor age distributions prior to Pangea formation at 330 Ma, because our plate motion model does not include any significant variability for the oceanic plates. The agreement with the observed present-day seafloor ages is expected, because they were used to derive the plate motion model (e.g., Lithgow-Bertelloni and Richards, 1998; Müller et al., 2008). However, we found the need to neglect or reduce the seafloor production at the ridge between Pacific and Chatham Rise Plates and the ridge along the Izanagi–Pacific plate boundary between 84 and 100 Ma to avoid too young seafloors in the western Pacific. This may result from the limited number of plate motion stages in the original plate motion model (e.g., Lithgow-Bertelloni and Richards, 1998) or too large plate motions during the Cretaceous Superchron between 80 and 120 Ma.

Based on the seafloor age distributions, we determined averaged oceanic heat flux (i.e., for seafloor younger than 160 Ma) and seafloor ages for the last 350 Ma (Fig. 2b). Our calculated averaged age of 64 Ma for the present-day seafloor is consistent with the observed (Müller et al., 1997; Xu et al., 2006). The averaged seafloor age is smallest at ~100 Ma ago after Pangea formation (Fig. 2b). The averaged seafloor age shows its second minimum at ~230 Ma ago, reflecting the opening of Tethys Ocean (Fig. 4f). The averaged seafloor age correlates well with the averaged oceanic heat flux that reaches maximum when the averaged age is minimal, confirming the control of lithospheric age on surface heat flux (Fig. 2b) (e.g., Lister, 1977). The averaged oceanic heat flux for the present-day is ~96 mW/m² (Fig. 2b), consistent with the observed 100 mW/m² (Pollack et al., 1993; Turcotte and Schubert, 2002). The averaged oceanic heat flux shows nearly the same time-dependence as the total surface heat flux (Fig. 2b), indicating that the oceanic heat flux predominates the total surface heat flux.

The area-age distributions at 350, 200, and 110 Ma ago and for the present-day all show an approximately triangular form (Fig. 5a). Although the triangular area-age distributions for 350 and 200 Ma ago simply reflect our assumed plate motions for the Pacific plates before 120 Ma, they are consistent with the area-age distribution for the present-day seafloor and inferences from observations of eustatic sea-level changes (e.g., Parsons, 1982). Finally, a half-space cooling model (e.g., Turcotte and Schubert, 2002) is also used to estimate surface heat flux q from ocean floors based on the seafloor age τ using $q = k\Delta T_l / \sqrt{\pi\kappa\tau}$, where k and κ are thermal conductivity and thermal diffusivity (Table 1), respectively, and ΔT_l is the temperature drop across the lithosphere and is determined directly from our convection model to be 1390 °C (Fig. 3b). The oceanic heat flux estimated from the cooling model closely follows the actual one but is ~6% smaller (Fig. 2b), and the difference may be due to sublithospheric small-scale convection (e.g., Davaille and Jaupart, 1994; Huang and Zhong, 2005).

3.2. CMB heat flux for case HF1

The global average CMB heat flux with time for case HF1 is shown in Fig. 2c, and the CMB heat flux and temperature distribution at 2835 km depth (i.e., 32 km above the CMB) at 330, 270, 180, 97, and 0 Ma are shown in Fig. 6. The present-day CMB heat flux is characterized by two low heat flux areas below Africa and the central Pacific, and a high heat flux girdle between them (Fig. 6i). This distribution of CMB heat flux arises because the hot African and Pacific chemical piles tend to insulate the core, while the cold downwellings elsewhere in the CMB

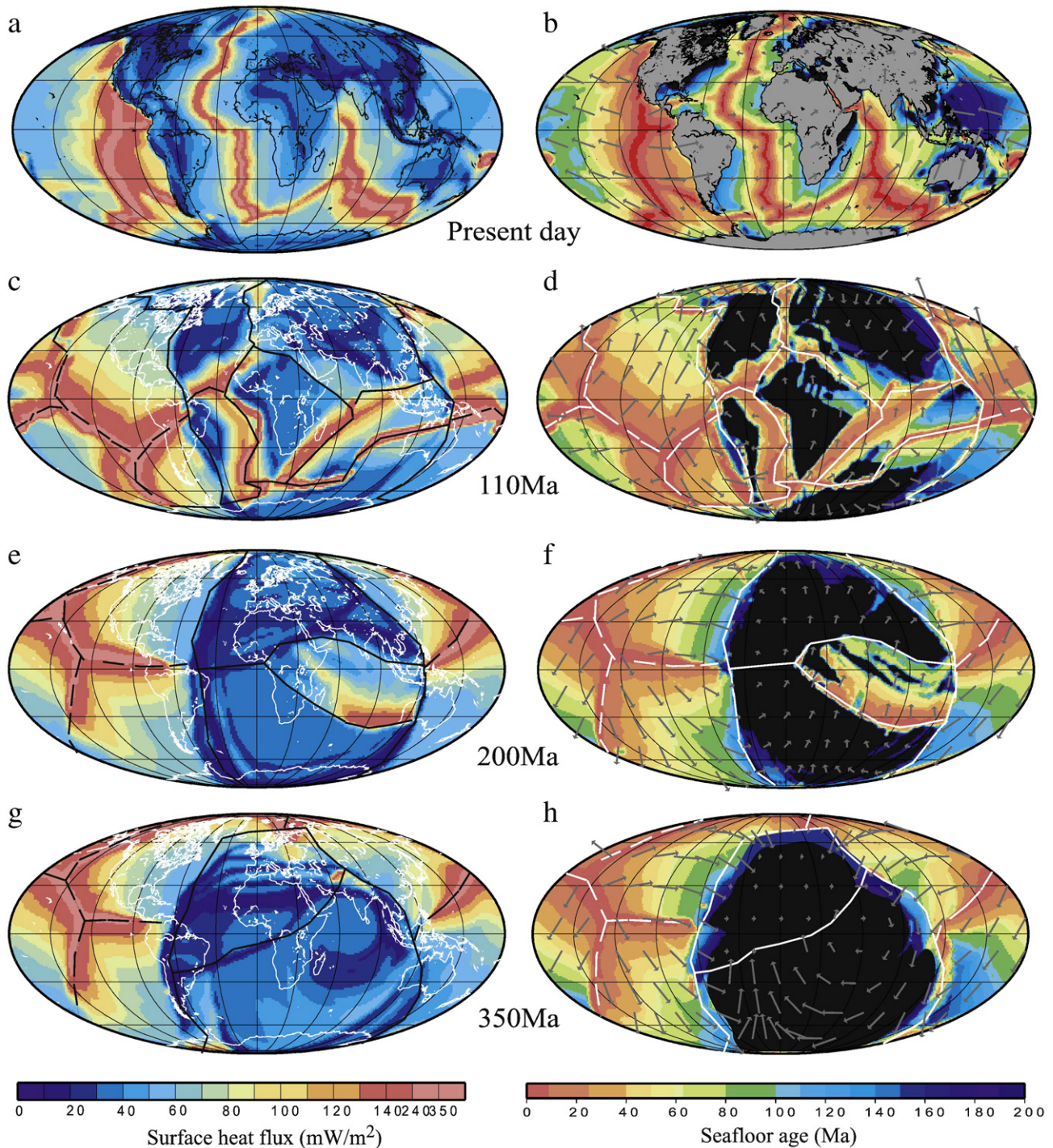


Fig. 4. Snapshots of the surface heat fluxes and seafloor ages for case HF1 for (a) the present day, (b) 110 Ma, (c) 200 Ma, and (d) 350 Ma ago. Seafloor age in black regions in the age maps is undefined. The arrows in left column of maps show the plate motions. Solid and dashed lines in Fig. 4c–h represent continental and oceanic plate boundaries, respectively. The coastlines for the present day are also shown in heat flux maps for reference.

regions (Fig. 6j) enhance the CMB heat flux. The present-day average CMB heat flux is 86 mW/m^2 or 13.3 TW in total. Overall, the CMB heat flux after Pangea formation shows two important features: the maximum between 110 Ma and 70 Ma ago and the minimum between 310 Ma and 240 Ma ago (Fig. 2c), and both features may be related to the surface tectonic events and hence surface heat flux. The CMB heat flux reaches a peak at 330 Ma and then decreases to a low valley at $\sim 310 \text{ Ma}$ ago, similar to the surface heat flux (Fig. 2b and c). From 310 to 240 Ma, the average CMB heat flux remains relatively low at $\sim 78 \text{ mW/m}^2$, but increases to 84 mW/m^2 at $\sim 210 \text{ Ma}$ ago (Fig. 2c). The

relatively low CMB heat flux after Pangea assembly may result from reduced subduction (e.g., the cessation of subduction between Gondwana and Laurussia) following Pangea assembly, while the subsequent increase in CMB heat flux may be caused by enhanced subduction associated with the opening of Tethys Ocean. Notice that the opening of Tethys Ocean causes a surface heat flux maximum at $\sim 240 \text{ Ma}$ ago (Fig. 2b). After 210 Ma, the CMB heat flux remains stable until $\sim 150 \text{ Ma}$ ago when it starts to increase to its highest value at $\sim 110 \text{ Ma}$ ago. The CMB heat flux remains high until it starts to decrease steadily at 70 Ma ago (Fig. 2c). Notice that the surface heat flux starts to

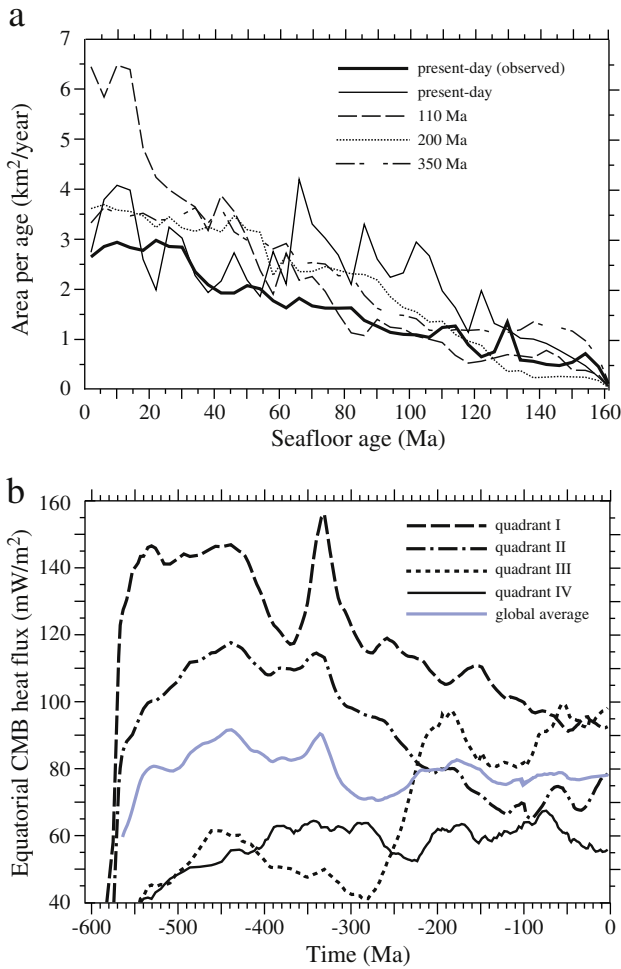


Fig. 5. Area–age distributions for the observed present-day seafloor (Müller et al., 1997) and modeled seafloor for the present-day, 110 Ma, 200 Ma and 350 Ma ago (a), and the averaged equatorial CMB heat fluxes within four quadrants as indicated in Fig. 6f. In Fig. 5a, the area–age distributions are computed for 4 Ma age bins. In Fig. 5b, the shaded curve is the global averaged equatorial heat as in Fig. 2d.

increase rapidly at ~170 Ma ago, is at its maximum between 120 Ma and 100 Ma ago, and starts to decrease at ~100 Ma ago (Fig. 2b). This suggests that the CMB heat flux is related to the surface heat flux and surface tectonics (Gait et al., 2008) but perhaps with ~30 Ma delay.

We now focus on the CMB heat flux and lower mantle structures in the equatorial regions because of their potential implications for the geodynamo process (Olson et al., 2010). The CMB heat flux in equatorial regions is computed within either 10° or 20° on either side of the equator. The equatorial CMB heat flux has two maxima at ~330 Ma and 180 Ma ago and two minima at ~270 Ma and ~100 Ma ago (Fig. 2d), all of which may be related to surface tectonics. The maximum equatorial CMB heat flux at 330 Ma is caused by the long-term convergence between Laurussia and Gondwana near the equator (Scotese, 2001) that leads to accumulation of cold slabs in the equatorial regions of the CMB (Fig. 6i and j). After Pangea is formed and the Laurussia–Gondwana convergence ends, the equatorial regions of the CMB below Pangea start to warm up, leading to reduced equatorial CMB heat flux between 310 and 260 Ma (Figs. 2d, 6g and h) and possibly also to the reduced total CMB heat flux during this period of time (Fig. 2c). This is evident in the equatorial CMB heat fluxes for four subdivisions of the equatorial regions (quadrants I and II in Fig. 5b are for CMB regions below Pangea).

The equatorial CMB heat flux gradually increases from 260 Ma to 180 Ma (Figs. 2d and 6e) because of the enhanced subduction and

convergence between the newly opening Tethys Ocean and Eurasia near the equator (Figs. 6f and 5b) (Scotese, 2001; Zhang et al., 2010). After 180 Ma, Pangea breakup initiates multiple continental plates, and particularly the reduced convergence between the Africa–India plate and Eurasia (Scotese, 2001) causes the equatorial CMB heat flux to decrease to a minimum at ~120 Ma ago and to remain low until ~90 Ma ago (Figs. 2d, 6c, d, and 5b). The increase of the equatorial CMB heat flux at ~90 Ma ago results from the northward acceleration of the Indian plate (Lithgow-Bertelloni and Richards, 1998) that causes a more intense subduction (Fig. 2d). The equatorial CMB heat flux starts to decrease at ~60 Ma ago (Fig. 2d), possibly reflecting the global trend in the CMB heat flux (Fig. 2c). It is interesting to note that the global CMB heat flux is at its peak between 110 and 70 Ma (Fig. 2c). The minimum equatorial CMB heat flux between 120 and 90 Ma (Fig. 2d) implies that the CMB heat flux in non-equatorial or high latitude regions must be significantly elevated during this period of time.

3.3. Influences of different parameters on the heat fluxes

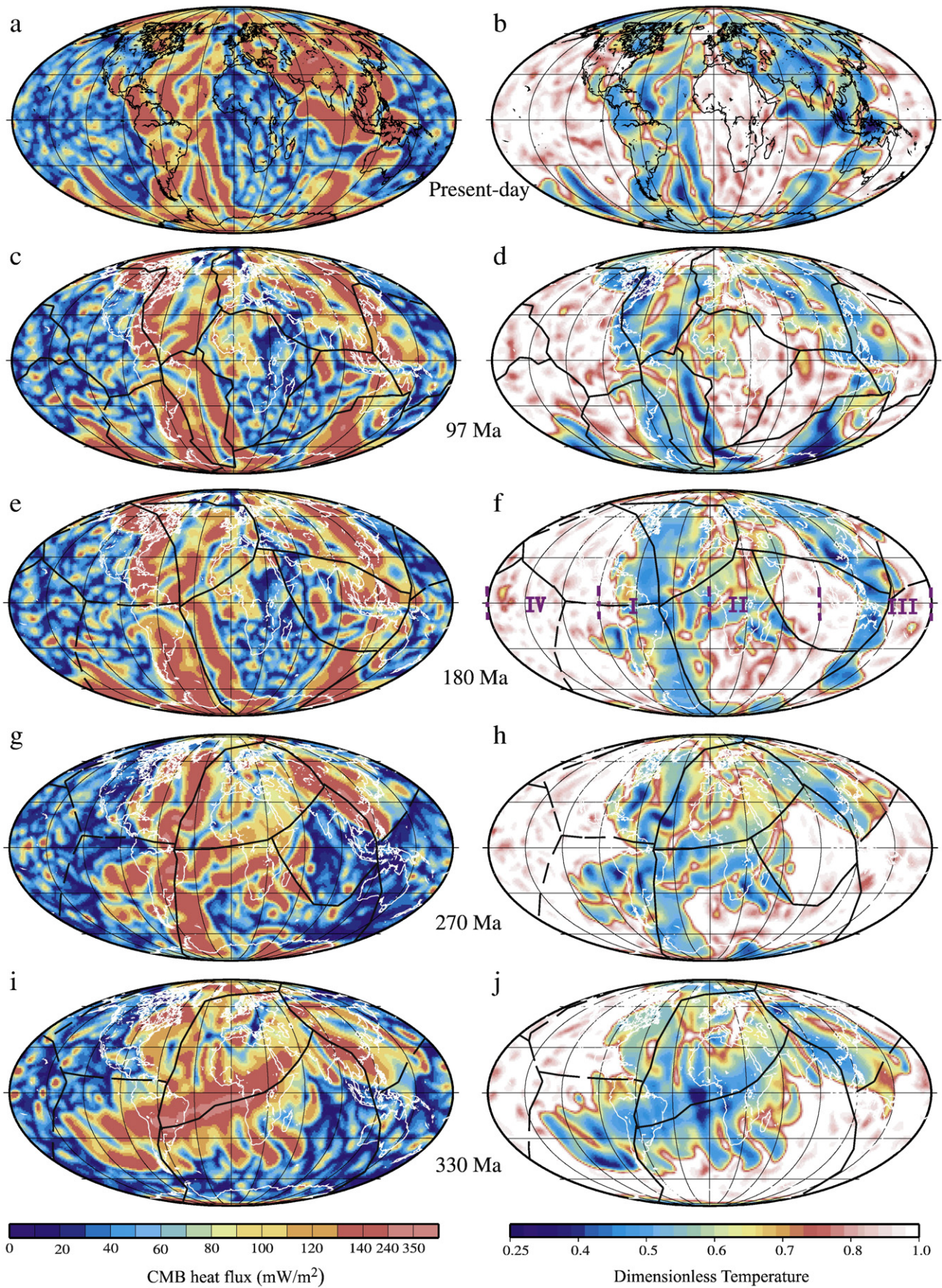
We now present five more cases (cases HF2–HF6 in Table 2) in which we remove the chemical layer, vary the viscosity structure, add the phase changes of Ringwoodite to perovskite and perovskite to post-perovskite, and increase the spreading rate for the Pacific oceanic plates, to examine their effects on the heat fluxes.

Case HF2 differs from case HF1 by removing the chemical layer above the CMB. The surface heat flux shows similar temporal variations to that of case HF1 (Fig. 7a), suggesting that the surface heat flux is mainly controlled by surface plate motions and is insensitive to the chemical layer above the CMB. However, without the chemical layer on the CMB, mantle temperature immediately above the CMB is significantly reduced (Fig. 3b), causing the average CMB heat flux to increase by ~18%, compared to that for case HF1 (Fig. 2c). Also the global and equatorial CMB heat fluxes for case HF2 shows very different temporal variations compared to case HF1 (Fig. 2c and d), again suggesting a significant role of chemical piles in the CMB heat flux. Although the present-day CMB heat flux distribution for case HF2 shows low heat fluxes beneath Africa and the central Pacific that are similar to that of case HF1, the spatial variations for case HF2 are much smaller (Fig. 8 and Supplementary Table 1).

A potentially important parameter that influences the response of the CMB heat flux to subducted slabs is the viscosity contrast between the upper and lower mantles. In case HF3, we reduce the lower mantle viscosity by a factor of three (Fig. 3a) to investigate its effects on the heat flux. It should be noted that the Rayleigh number Ra for case HF3 is reduced by a factor two to keep a similar convective vigor to case HF1 (Table 2). Except for these two changes, case HF3 is identical to case HF1. The temporal and spatial variations of the surface heat flux for case HF3 remain similar to those for case HF1 (Fig. 7a). Although the global and equatorial CMB heat fluxes show similar temporal variations to those for case HF1, they are ~10% higher than those for case HF1 (Fig. 7b and c). The enhanced CMB heat fluxes result from more vigorous convection in the lower mantle due to the reduced viscosity. Importantly, the equatorial CMB heat flux also shows two minima at around 270 Ma and 100 Ma ago (Fig. 7c).

Case HF4 has a perovskite to post-perovskite phase change at depth 2700 km (Table 1), and is otherwise identical to case HF1. The surface heat flux is similar to that for case HF1 (Fig. 7a). The global and equatorial CMB heat fluxes show similar temporal variations to those for case HF1 but with ~16% higher amplitude (Fig. 7b and c). Higher CMB heat fluxes arise because the exothermic phase change enhances convective instability near the CMB (e.g., Matyska and Yuen, 2005; Nakagawa and Tackley, 2004, 2008).

Case HF5 included a Ringwoodite to perovskite phase change at a 670-km depth (Table 1). The endothermic phase change leads to the occasional ponding of cold slabs (hot upwellings) above (below) the phase boundary (Christensen and Yuen, 1985), as evident in the radial



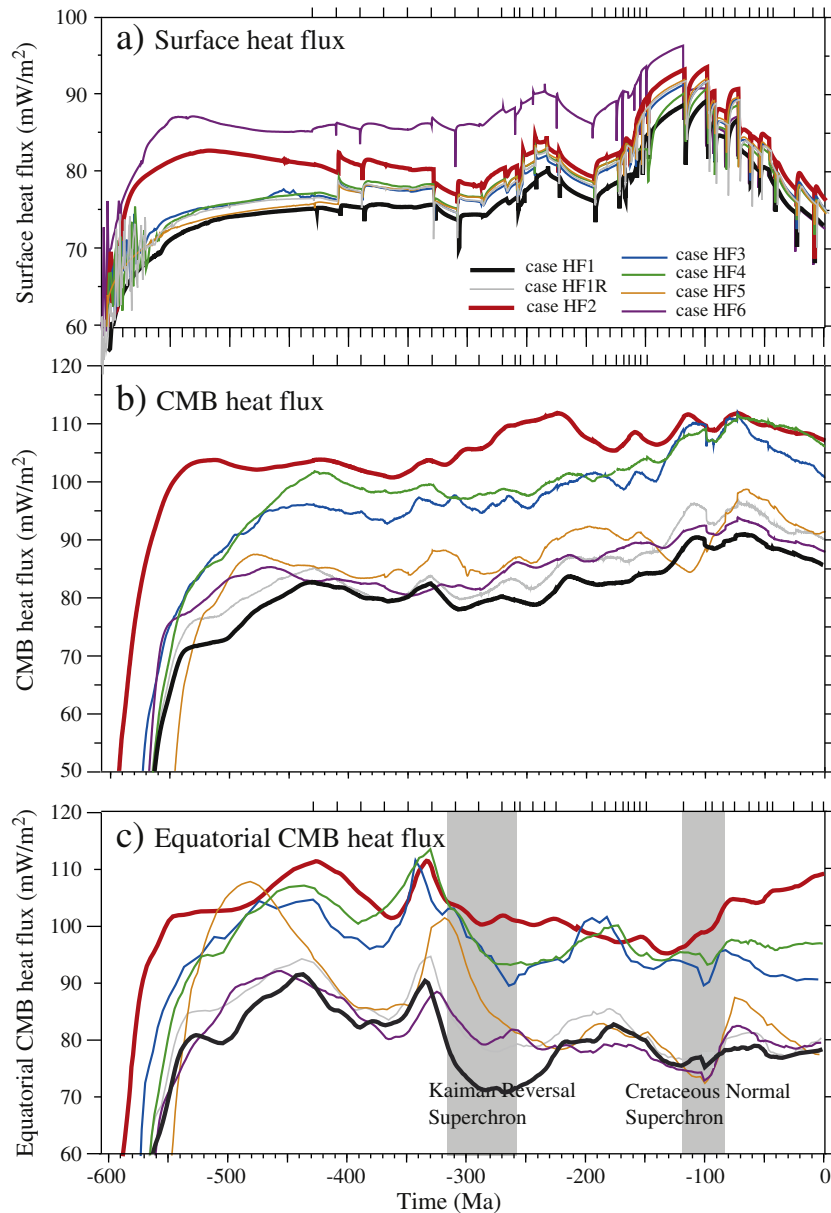


Fig. 7. Time dependence of the averaged surface (a), global CMB (b), and equatorial CMB (c) heat fluxes for all the cases. The two shaded zones in Fig. 8c represent the time periods for the Kaiman and Cretaceous Superchrons.

temperature profile (Fig. 3b). The ponded materials may suddenly flush through the phase boundary, thus enhancing the temporal variability of the CMB heat flux (Christensen and Yuen, 1985; Machetel and Weber, 1991). This can be seen in the time dependences of global and equatorial CMB heat fluxes (Fig. 7b and c), although the surface heat flux remains largely unchanged relative to case HF1 (Fig. 7a). Interestingly, the global CMB heat flux for case HF5 displays a strong minimum at ~110 Ma (Fig. 7b). The equatorial CMB heat flux still shows two minima at ~230 Ma and ~100 Ma, but the first minimum occurs ~40 Ma later than that in other cases with chemical piles (Fig. 7c).

A significant uncertainty in our models is the plate motions in the Pacific hemisphere before 120 Ma. Zhang et al. (2010) found that plate

configurations in the Pacific hemisphere have relatively small effects on long-wavelength mantle structures, provided that the hemisphere is predominated by spreading centers. It is important to investigate the influence of different oceanic plate motions on the heat flux, especially the surface heat flux. In case HF6, the averaged plate motion for the Pacific hemisphere before 120 Ma is increased to 11 cm/yr from the 8 cm/yr value in case HF1 (Fig. 2a), and otherwise this case is identical to case HF1. The increased plate motions lead to ~13% higher surface heat flux than that for case HF1 before 120 Ma, but the surface heat flux after 120 Ma is nearly identical to that for case HF1 (Fig. 2b), further indicating the strong influence of plate motions on the surface heat flux. However, the increased plate motions have relatively small effects on the CMB heat flux (Fig. 7b and c). The equatorial CMB heat

Fig. 6. Snapshots of the CMB heat fluxes (left column) and temperatures at 2835 km depth (right column) for case HF1 at (a, b) the present day, (c, d) 97 Ma, (e, f) 180 Ma, (g, h) 270 Ma, and (i, j) 330 Ma ago. The two white lines in each map represent 10°S and 10°N latitudes for which our equatorial CMB heat fluxes are computed. The purple lines in Fig. 6f mark the four quadrants in which equatorial heat fluxes are quantified and presented in Fig. 5b.

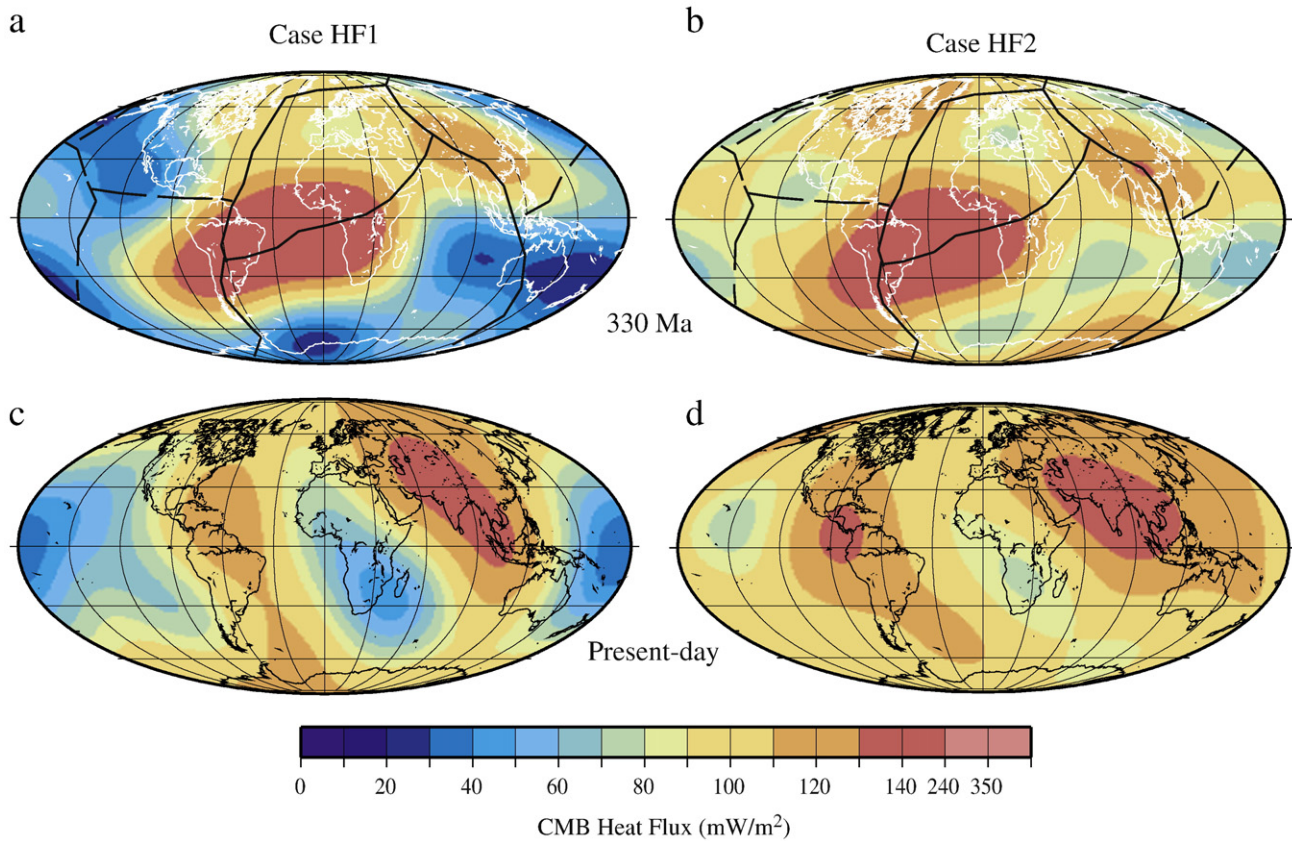


Fig. 8. Snapshots of the long-wavelength (i.e., the first 4 spherical harmonic degrees and orders) components of the CMB heat fluxes for cases HF1 (left column) and HF2 (right column) at (a, b) 330 Ma ago and (c, d) the present day. The spherical harmonic coefficients of these components are shown in supplemental Table 1.

flux for case HF6 also shows two lows at 282 and 96 Ma ago, although the high heat flux between these two lows is subdued (Fig. 7c).

4. Discussions

Our study represents the first attempt to reconstruct Earth's surface and CMB heat flux associated with Pangea assembly and breakup since the early Paleozoic using 3-D spherical mantle convection models. Our results confirm the dominant role of plate motions and seafloor ages in controlling the surface heat flux (e.g., Lister, 1977; Parsons, 1982; Stein and Lowman, 2010), and other processes such as sublithospheric small-scale convection only have secondary roles. Our reference model (i.e., case HF1), using a plate motion model for the last 450 Ma (Zhang et al., 2010), reproduces well the present-day surface heat flux in both spatial distribution and amplitude. The most robust and significant result on the surface heat flux from our reference model is ~16% of surface heat flux increase from 190 Ma to 120 Ma ago associated with Pangea breakup and the subsequent ~18% decrease of surface heat flux for the last 100 Ma (Fig. 2b). This indicates that the present-day heat flux is only slightly lower than that at ~200 Ma ago or before Pangea breakup. Our models show that the assembly and continuous existence of supercontinent Pangea may not affect global surface heat flux (Fig. 2b), provided that oceanic plate motions are kept constant. In fact, the opening of the Tethys Ocean causes larger variations in the global surface heat flux than the Pangea assembly.

This temporal variation in surface heat flux correlates well with the average seafloor ages (Fig. 2b). Two minima in the average seafloor age occur at 100 and 240 Ma ago, reflecting the young seafloors resulting from the Pangea breakup and the opening of the Tethys Ocean, respectively. The area-age distributions in our reference model all show approximately triangular forms (Fig. 5a). However, compared with the present-day observation, the seafloor production in our

model is too large between 70 and 110 Ma. Also, the area-age distribution curve for 110 Ma ago shows significantly larger seafloor production for the 0–15 Ma age band than other ages (Fig. 5a). This most likely reflects the large Pacific plate motions between 80 and 120 Ma used in the plate motion model (Lithgow-Bertelloni and Richards, 1998). How to improve the fit to the present-day area-age distribution is an important future research topic.

Our surface heat flux and seafloor age results necessarily depend on our plate motion model, particularly the assumed plate motions for the Pacific plates before 120 Ma that in our reference case are assumed to resemble the plate configurations at 120 Ma with a fixed averaged speed of 8 cm/yr (e.g., Zhang et al., 2010). If the averaged plate motion for the Pacific plates before 120 Ma is increased to 11 cm/yr (case HF6), the surface heat flux before 120 Ma becomes much higher, while the heat flux for the last 120 Ma remains the same, compared to the reference case. This leads to a pre-Pangea breakup heat flux that is ~16% higher than the present-day value (Fig. 2b). Eustatic sea-level changes have been used to constrain surface heat flux changes (e.g., Turcotte and Burke, 1978), because both are mainly controlled by mean seafloor ages (Turcotte and Schubert, 2002). Eustatic sea-level changes show a ~150 m rise from 200 to 100 Ma and then a fall for the last 100 Ma to the pre-200 Ma level (Haq et al., 1987; Haq and Schutter, 2008; Miller et al., 2005; Watts and Steckler, 1979). This temporal variation in eustatic sea-level changes is similar to that for the surface heat flux from our reference case but not to that from case HF6 with larger plate motions. Based on the relationship between the eustatic sea-level and surface heat flux changes (Turcotte and Schubert, 2002), we suggest that the eustatic sea level changes after Pangea formation to the first order support the predicted time evolution of surface heat flux from our reference model and the assumed plate motion model for the Pacific plates before 120 Ma used in that reference case.

Time evolution of surface heat flux for the last 140 Ma has also been estimated based on reconstructed seafloor age distributions (e.g., Becker et al., 2009; Loyd et al., 2007). The rapid decrease in surface heat flux for the last 120 Ma from our models is consistent with Loyd et al. (2007) and Becker et al. (2009), but is in disagreement with the Grigne et al.'s (2005) proposal that the present-day heat flux is at its maximum. Becker et al. (2009) also suggested that the surface heat flux increases from Pangea breakup to ~120 Ma ago, based on an assumed periodicity in the seafloor production. Korenaga (2007) reiterated the argument of eustatic sea level and surface heat flux changes by Turcotte and Schubert (2002) that the surface heat flux before Pangea breakup should be comparable to the present-day value. Assuming that seafloor age-area distribution for the last 180 Ma resembles that for the present-day, Cogné et al. (2006) found that the averaged seafloor age is uniformly small from 40 Ma to 100 Ma ago with a minimum at 50 Ma, while the averaged seafloor age between 120 and 180 Ma ago is similar to that for the present-day. Although Cogné et al. (2006) only used the averaged seafloor ages to explain the eustatic sea level changes and did not attempt to convert the ages to surface heat flux, their results also imply that the surface heat flux at 180 Ma ago is similar to the present-day value and that the surface heat flux is maximum between 100 Ma and 50 Ma ago. While this result is broadly consistent with ours, the occurrence of minimal averaged seafloor age at 50 Ma ago in Cogné et al. (2006) is significantly later than that in our model (i.e., at 100 Ma ago).

Our model calculations with dense chemical piles above the CMB show consistently that surface plate motions, by organizing mantle convection structure in the lower mantle, have significant effects on both the magnitude and distribution of the CMB heat flux. Our reference case shows that for the present-day, the CMB heat flux is significantly lower below the African and Pacific chemical piles than the surrounding regions, because the hot chemical piles tend to insulate the core. This CMB heat flux pattern has been used in geodynamo modeling (e.g., Aubert et al., 2008; Olson and Glatzmaier, 1996). Global CMB heat flux from most of our models displays a maximum from 120 to 70 Ma ago (Fig. 7b), while the equatorial CMB heat flux displays two clear minima at ~270 Ma and ~100 Ma ago (Fig. 7c), all of which may be related to surface tectonic events, as discussed in the result section.

Reduced CMB heat flux or equatorial CMB heat flux may stabilize geomagnetic polarities and lead to superchrons (Olson et al., 2010). Over our modeled geological time periods, two superchrons, the Kiaman and Cretaceous Superchrons, occurred during the time periods of 316–262 Ma and 118–83 Ma, respectively. We found that the two minima in the equatorial CMB heat flux at ~270 Ma and ~100 Ma ago and the maximum in the global CMB heat flux at ~100 Ma coincide approximately with the two superchrons. It should be noted that during the Cretaceous Superchron (i.e., 80–120 Ma ago), the maximum global CMB heat flux and the minimal equatorial CMB heat flux from our models suggest that the CMB heat flux in the polar or high latitude regions must be elevated significantly. How such a CMB heat flux pattern affects geomagnetic polarity reversals has interesting implications for the Cretaceous superchron. Taking into account of recent geodynamo studies by Olson et al. (2010), we suggest that the CMB heat flux from our models may help explain the Cretaceous and Kiaman superchrons.

Finally, our models suggest that the dense chemical piles above the CMB have the strongest effect on the CMB heat flux. The removal of chemical piles (case HF2) leads to more smooth spatial variations with smaller amplitudes in the CMB heat flux, although the long-wavelength patterns remain similar (Fig. 8). Using similar convection models, Lassak et al. (2010) found that the chemical piles do not affect the amplitude and patterns of CMB dynamic topography at long-wavelengths (spherical harmonic degrees and orders less than 4). This is similar to our finding here for the CMB heat flux except that we found that the amplitudes differ significantly (Fig. 8 and Supplementary Table 1). A perovskite to post-perovskite phase change near the CMB (case HF4) and a reduced viscosity contrast between the upper

and lower mantles (case HF3) also greatly enhance the CMB heat flux magnitude, because they enhance the relative convective vigor in the lower mantle. However, the temporal variations of global and equatorial CMB heat fluxes from our models appear to be rather robust, provided that the models include dense chemical piles above the CMB. It should be pointed out that numerical resolution has only relatively small effects on our results, as shown by case HF1R and that a reduced numerical resolution (12×48^3 elements, Table 2) reproduces the temporal and spatial variations in the heat flux results for case HF1 but with a slightly (~5%) larger amplitude (Fig. 7).

5. Conclusions

We have formulated 3-D spherical models of mantle convection with imposed plate motion history to reconstruct temporal evolution of surface and CMB heat flux since the Early Paleozoic and Pangea era. Our model results can be summarized as follows.

- 1) Our models reproduce well present-day observations of the surface heat flux and seafloor age distributions. The models confirm that the surface heat flux is mainly controlled by seafloor age and oceanic plate motions, while indicating a relatively small role of sublithospheric small-scale convection in the global surface heat flux.
- 2) The assembly process of supercontinent Pangea and the existence of Pangea may not have significant effects on the surface heat flux. However, Pangea breakup has major influences on the surface heat flux that increases by ~16% from 190 Ma to 120 Ma ago associated with Pangea breakup and decreases subsequently by ~18% for the last 100 Ma, as global plate motions slow down. This indicates that the present-day heat flux is similar to that at ~200 Ma ago or before Pangea breakup. While the amount of surface heat flux increase before 120 Ma depends on our assumed plate motions for the Pacific plates, this temporal variation is consistent with the eustatic sea-level changes since Pangea assembly.
- 3) Surface tectonics and plate motions, by influencing the dynamics of subducted slabs in the lower mantle, have significant effects on temporal and spatial distributions of the CMB heat flux. Our models show that the present-day CMB heat flux is relatively low below the African and Pacific superplumes but is high elsewhere due to subducted slabs. However, the amplitude of these heat flux variations is significantly larger when the chemical piles exist above the CMB.
- 4) While our models with the chemical piles above the CMB consistently predict a maximum global CMB heat flux between 110 Ma and 70 Ma ago, the models also show that CMB heat flux in the equatorial regions is relatively low around 270 Ma and 100 Ma ago. We note that these two minima in the equatorial CMB heat flux coincide with the Kiaman Superchron and Cretaceous Superchron, and suggest that our CMB heat flux results may help explain the occurrence of the superchrons.

Acknowledgments

This work is supported by the U.S. National Science Foundation Grants EAR-1015669 and EAR-0855712, and the David and Lucile Packard Foundation. The CIG is thanked for distributing the software CitcomS that is used in this study.

Appendix A. Supplementary data

Supplementary data to this article can be found online at doi:10.1016/j.epsl.2011.04.001.

References

- Aubert, J., Amit, H., Hulot, G., Olson, P., 2008. Thermochemical flows couple the Earth's inner core growth to mantle heterogeneity. *Nature* 454, 758–761.
- Becker, T.W., Conrad, P.C., Buffett, B.A., Müller, R.D., 2009. Past and present seafloor age distributions and the temporal evolution of plate tectonic heat transport. *Earth Planet. Sci. Lett.* 278, 233–242.
- Bercovici, D., 2003. The generation of plate tectonics from mantle convection. *Earth Planet. Sci. Lett.* 205, 107–121.
- Buffett, B.A., 2002. Estimates of heat flow in the deep mantle based on the power requirements for the geodynamo. *Geophys. Res. Lett.* 29, 1566. doi:10.1029/2001GL014649.
- Bull, A.L., McNamara, A.K., Ritsema, J., 2009. Synthetic tomography of plume clusters and thermochemical piles. *Earth Planet. Sci. Lett.* 278, 152–162.
- Bunge, H.-P., 2005. Low plume excess temperature and high core heat flux inferred from non-adiabatic geotherms in internally heated mantle circulation models. *Phys. Earth Planet. Inter.* 153, 3–10.
- Bunge, H.-P., Richards, M.A., Lithgow-Bertelloni, C., Baumgardner, J.R., Grand, S., Romanowicz, B., 1998. Time scales and heterogeneous structure in geodynamic earth models. *Science* 280, 91–95.
- Cande, S.C., Kent, D.V., 1995. Revised calibration of the geomagnetic polarity timescale for the Late Cretaceous and Cenozoic. *J. Geophys. Res.* 100, 6093–6095.
- Christensen, U., Yuen, D.A., 1985. Layered convection induced by phase transitions. *J. Geophys. Res.* 90, 10,291–10,300.
- Cogné, J.P., Humler, E., 2004. Temporal variations of oceanic spreading and crustal production rates during the last 180 My. *Earth Planet. Sci. Lett.* 227, 427–439.
- Cogné, J.-P., Humler, E., Courtillot, V., 2006. Mean age of oceanic lithosphere drives eustatic sea-level change since Pangea breakup. *Earth Planet. Sci. Lett.* 245, 115–122.
- Conrad, C.P., Gurnis, M., 2003. Mantle flow, seismic tomography and the breakup of Gondwanaland: integrating mantle convection backwards in time. *Geochemistry Geophysics Geosystems* 4, 1031. doi:10.1029/2001GC000299.
- Davaille, A., Jaupart, C., 1994. The onset of thermal convection in fluids with strongly temperature-dependent viscosity and the oceanic mantle. *J. Geophys. Res.* 99, 19853.
- Davies, G.F., 1988. Ocean bathymetry and mantle convection: 1. Largescale flow and hotspots. *J. Geophys. Res.* 93, 10,467–10,480.
- Davies, G.F., 1999. *Dynamic Earth: Plates, Plumes and Mantle Convection*. Cambridge Univ. Press, Cambridge, U. K. 470 pp.
- Gait, A.D., Lowman, J.P., Gable, C.W., 2008. Time-dependence in 3D mantle convection models featuring evolving plates: the effect of lower mantle viscosity. *J. Geophys. Res.* Vol. 113. doi:10.1029/2007JB005538 B08409.
- Grigne, C., Labrosse, S., Tackley, P.J., 2005. Convective heat transfer as a function of wavelength: implications for the cooling of the Earth. *J. Geophys. Res.* 110, B03409. doi:10.1029/2004JB003376.
- Hager, B.H., Richards, M.A., 1989. Long-wavelength variations in the Earth's geoid: physical models and dynamic implications. *Philos. Trans. R. Soc. London. Ser. A* 328, 309–327.
- Haq, B.U., Schutter, S.R., 2008. A chronology of Paleozoic sea-level changes. *Science* 322, 64–68.
- Haq, B.U., Hardenbol, J., Vail, P.R., 1987. Chronology of fluctuating sea levels since the Triassic. *Science* 235, 1156–1167.
- Heller, P.L., Anderson, D.L., Angevine, C.L., 1996. Is the middle Cretaceous pulse of rapid sea-floor spreading real or necessary? *Geology* 24, 491–494.
- Hernlund, J.W., Thomas, C., Tackley, P.J., 2005. A doubling of the post-perovskite phase boundary and structure of the Earth's lowermost mantle. *Nature* 434, 882–886.
- Huang, J.S., Zhong, S.J., 2005. Sublithospheric small-scale convection and its implications for residual topography at old ocean basins and the plate model. *J. Geophys. Res.* 110, B05404. doi:10.1029/2004JB003153.
- King, S.D., Lowman, J.P., Gable, C.W., 2002. Episodic tectonic plate reorganizations driven by mantle convection. *Earth Planet. Sci. Lett.* 203, 83–91. doi:10.1016/S0012-821X(02)00852-X.
- Korenaga, J., 2007. Eustasy, supercontinental insulation, and the temporal variability of terrestrial heat flux. *Earth Planet. Sci. Lett.* 257, 350–358.
- Lassak, T.M., McNamara, A.K., Garnero, E.J., Zhong, S.J., 2010. Core–mantle boundary topography as a possible constraint on lower mantle chemistry and dynamics. *Earth Planet. Sci. Lett.* 289, 232–241. doi:10.1016/j.epsl.2009.11.012.
- Lay, T., Hernlund, J., Buffett, B.A., 2008. Core–mantle boundary heat flux. *Nature Geoscience* 1, 25–32.
- Leng, W., Zhong, S.J., 2008. Constraints on plume heat flux and plume excess temperature. *J. Geophys. Res.* 113, B04408. doi:10.1029/2007JB005155.
- Lister, C.R.B., 1977. Qualitative models of spreading center processes, including hydrothermal penetration. *Tectonophysics* 37, 203–218.
- Lithgow-Bertelloni, C., Richards, M.A., 1998. Dynamics of Cenozoic and Mesozoic plate motions. *Rev. Geophys.* 36, 27–78.
- Liu, L.J., Spasojevic, S., Gurnis, M., 2008. Reconstructing Farallon Plate subduction beneath North America back to the Late Cretaceous. *Science* 322, 934–938.
- Lloyd, S.J., Becker, T.W., Conrad, C.P., Lithgow-Bertelloni, C., Corsetti, F.A., 2007. Time-variability in Cenozoic reconstructions of mantle heat flow: plate tectonic cycles and implications for Earth's thermal evolution. *Proceed. Nat. Acad. Sci.* 104, 14266–14271.
- Machetel, P., Weber, P., 1991. Intermittent layered convection in a model mantle with an endothermic phase change at 670 km. *Nature* 350, 55–57.
- Matyska, C., Yuen, D.A., 2005. The importance of radiative heat transfer on superplumes in the lower mantle with the new post-perovskite phase change. *Earth Planet. Sci. Lett.* 234, 71–81.
- McNamara, A.K., Zhong, S.J., 2005. Thermochemical structures beneath Africa and the Pacific Ocean. *Nature* 437, 1136–1139. doi:10.1038/nature04066.
- Miller, K.G., Kominz, M.A., Browning, J.V., Wright, J.D., Mountain, G.S., Katz, M.E., Sugarman, P.J., Cramer, B.S., Christie-Blick, N., Pekar, S.F., 2005. The Phanerozoic record of global sea-level change. *Science* 312, 1293–1298.
- Moucha, R., Forte, A.M., Rowley, D.B., Mitrovica, J.X., Simmons, N.A., Grand, S.P., 2008. Mantle convection and the recent evolution of the Colorado Plateau and the Rio Grande Rift valley. *Geology* 36, 439–442.
- Müller, R.D., Roest, W.R., Royer, J.-Y., Gahagan, L.M., Sclater, J.G., 1997. Digital isochrons of the world's ocean floor. *J. Geophys. Res.* 102, 3211–3214.
- Müller, R.D., Gaina, C., Roest, W.R., 2008. Age, spreading rates, and spreading asymmetry of the world's ocean crust. *Geochemistry Geophysics Geosystems* 9, Q04006. doi:10.1029/2007GC001743.
- Nakagawa, T., Tackley, P.J., 2004. Effects of a perovskite–post perovskite phase change near the core–mantle boundary in compressible mantle convection. *Geophys. Res. Lett.* 31, L16611.
- Nakagawa, T., Tackley, P.J., 2008. Lateral variations in CMB heat flux and deep mantle seismic velocity caused by a thermal–chemical–phase boundary layer in 3D spherical convection. *Earth Planet. Sci. Lett.* 271, 348–358.
- Olson, P., Glatzmaier, G.A., 1996. Magneto-convection and thermal coupling of the Earth's core and mantle. *Philos. Trans. R. Soc. Lond. A* 354, 1413–1424.
- Olson, P., Coe, R.S., Driscoll, P.E., Glatzmaier, G.A., Roberts, P.H., 2010. Geodynamo reversal frequency and heterogeneous core–mantle boundary heat flow. *Phys. Earth Planet. Interiors* 180, 66–79.
- Parsons, B., 1982. Causes and consequences of the relation between area and age of the ocean floor. *J. Geophys. Res.* 87, 289–302.
- Pollack, H.N., Hurter, S.J., Johnson, J.R., 1993. Heat flow from the earth's interior – analysis of the global data set. *Rev. Geophys.* 31 (3), 267–280.
- Ricard, Y., Richards, M.A., Lithgow-Bertelloni, C., Lestunff, Y., 1993. A geodynamic model of mantle mass heterogeneities. *J. Geophys. Res.* 98, 21,895–21,909. doi:10.1029/93JB02216.
- Rowley, D., 2002. History of plate Creation 180 Ma to present. *Geological Society America Bulletin* 114, 927–933.
- Safonova, I., Utsonomiya, A., Kojima, S., Nakae, S., Tomurtogoo, O., Filippov, A.N., Koizumi, K., 2009. Pacific superplume-related oceanic basalts hosted by accretionary complexes of Central Asia. *Russian Far East Japan Gondwana Research* 16, 587–608.
- Scotese, C.R., 2001. *Atlas of Earth History* (2001), PALEOMAP Progress Report 90–0497. Dept. of Geol., Univ. of Tex. at Arlington, Texas.
- Sleep, N.H., 1990. Hotspots and mantle plumes: some phenomenology. *J. Geophys. Res.* 95, 6715–6736.
- Stein, C., Lowman, J.P., 2010. Response of mantle heat flux to plate evolution. *Geophys. Res. Lett.* Vol. 37. doi:10.1029/2010GL045283 L24201.
- Turcotte, D.L., Burke, K., 1978. Sea-level changes and the thermal structures of the Earth. *Earth Planet. Sci. Lett.* 41, 341–346.
- Turcotte, D.L., Schubert, G., 2002. *Geodynamics*. Cambridge University Press, Second Edition. 456 pp.
- Watts, A.B., Steckler, M.S., 1979. Subsidence and Eustasy at the continental margin of eastern North America. *Deep Drilling Results in the Atlantic Ocean: Continental Margins and Paleoenvironment, Maurice Ewing Series, V. 3*, American Geophysical Union, pp. 218–234.
- Wen, L., Anderson, D.L., 1995. The fate of the slabs inferred from seismic tomography and 130 Ma subduction. *Earth Planet. Sci. Lett.* 133, 185–198.
- Xu, X., Lithgow-Bertelloni, C., Conrad, C.P., 2006. Global reconstructions of Cenozoic seafloor ages: implications for bathymetry and sea level. *Earth Planet. Sci. Lett.* 243, 552–564.
- Zhang, N., Zhong, S.J., Leng, W., Li, Z.X., 2010. A model for the evolution of the Earth's mantle structure since the Early Paleozoic. *J. Geophys. Res.* 115. doi:10.1029/2009JB006896.
- Zhong, S.J., 2006. Constraints on thermochemical convection of the mantle from plume heat flux, plume excess temperature and upper mantle temperature. *J. Geophys. Res.* 111, B04409. doi:10.1029/2005JB003972.
- Zhong, S.J., Zuber, M.T., Moresi, L., Gurnis, M., 2000. Role of temperature-dependent viscosity and surface plates in spherical shell models of mantle convection. *J. Geophys. Res.* 105, 11063–11082.
- Zhong, S.J., McNamara, A.K., Tan, E., Moresi, L., Gurnis, M., 2008. A benchmark study on mantle convection in a 3-D spherical shell using CitcomS. *Geochemistry Geophysics Geosystems* 9, Q10017. doi:10.1029/2008GC002048.
- Zhong, S.J., Zhang, N., Li, Z.X., Roberts, J.H., 2007. Supercontinent cycles, true polar wander, and very long wavelength mantle convection. *Earth Planet. Sci. Lett.* 261, 551–564. doi:10.1016/j.epsl.2007.07.049.